ACS APPLIED MATERIALS & INTERFACES

Research Article

www.acsami.org

Highly Efficient Iodide/Triiodide Dye-Sensitized Solar Cells with Gel-Coated Reduce Graphene Oxide/Single-Walled Carbon Nanotube Composites as the Counter Electrode Exhibiting an Open-Circuit Voltage of 0.90 V

Huiqin Zheng,[†,‡,§] Chin Yong Neo,[†,§] and Jianyong Ouyang*[,†]

[†]Department of Materials and Engineering, National University of Singapore, Singapore 117574

[‡]School of Materials Science and Engineering, Tongji University, Shanghai, 201804, China

Supporting Information

ABSTRACT: To increase the open-circuit voltage (V_{oc}) of dye-sensitized solar cells (DSCs), it is crucial to enhance the photovoltaic efficiency of DSCs. Here, we report an effective method to significantly improve the V_{oc} and photovoltaic efficiency of DSCs by using gel-coated composites of reduced graphene oxide (rGO) and single-walled carbon nanotubes (SWCNTs) as the counter electrode. Gel-coated rGO-SWCNT composites outperform Pt, rGO and SWCNTs in catalyzing the reduction of I_3^- and functioning as the counter electrode of DSCs. The V_{oc} and power conversion efficiency (PCE) are 0.86 V and 8.37% for fresh DSCs with the composite of 80 wt % rGO and 20 wt % SWCNTs, significantly higher than those (V_{oc} = 0.77 V, PCE = 7.79%) of control DSCs with Pt fabricated by pyrolysis as the counter electrode. The V_{oc} value of DSCs with rGO-SWCNT composites as the counter electrode further increases to 0.90 V after one week. The high V_{oc} and PCE are ascribed to the synergetic effects of rGO and SWCNTs in reducing the overpotential of the I_3^- reduction. RGO with high specific surface area can have high electrocatalytic activity, whereas SWCNTs give rise to high conductivity for the composites and facilitate the penetration of the redox species into rGO sheets by preventing the agglomeration of the rGO sheets. To the best of our knowledge, this is the first time to report iodide/triiodide DSCs with both high V_{oc} and PCE.

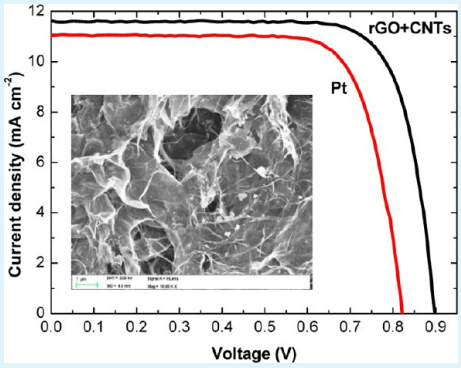

KEYWORDS: *dye-sensitized solar cells, reduced graphene oxide, carbon nanotubes, electrocatalysis*

1. INTRODUCTION

Dye-sensitized solar cells (DSCs) are regarded as the next-generation solar cells because of their low fabrication cost and decent power conversion efficiency (PCE).[1−6] PCE of more than 12% was recently reported on DSCs with Co complexes as the redox species in the electrolyte.[7] A DSC usually consists of a photoanode impregnated with dye, a counter electrode and electrolyte containing redox species between the two electrodes. Iodide/triiodide are a popular redox couple in the electrolyte of DSCs. The photon-to-electricity conversion of a DSC includes five key steps. (1) A photon absorbed by a dye molecule can stimulate the transition of an electron from the highest occupied molecular orbital (HOMO) to the lowest unoccupied molecular orbital (LUMO) of the dye molecule, when the photon energy is equivalent to or higher than the bandgap between the HOMO and LUMO. (2) The electron on the LUMO of the dye molecule transfers to the conduction band of the TiO_2 working electrode. (3) The electrons transport along the TiO_2 layer to the external circuit. (4) The dye molecule regenerates by gaining an electron from iodide, $2dye^+ + 3I^- \rightarrow dye^0 + I_3^-$. (5) The redox species transport in the electrolyte, and they regenerate on the counter electrode as a result of the reduction of triiodide, $I_3^- + 2e^- \rightarrow 3I^-$. All the steps can significant affect the photovoltaic efficiency of DSCs. Both the short-circuit current (J_{sc}) and the open-circuit voltage (V_{oc}) strongly depends on the energy levels of the dye molecules. In principle, the V_{oc} value can be close to the bandgap of the dye molecules. But the V_{oc} value of I^-/I_3^- DSCs rarely reaches half of the bandgap of the dyes, which is around 1.6 eV. It has been realized that the low V_{oc} value may be the most crucial reason for the overall device efficiency of DSCs. V_{oc} is determined by the difference between the quasi-Fermi level (E_{Fn}) of the TiO_2 working electrode and the redox potential (E_{redox}) of the redox species in the electrolyte.[7,8] Thus, efforts to improve V_{oc} have been focused on shifting E_{Fn} of TiO_2 upward or E_{redox} of the redox species downward. Methods to shift the E_{Fn} upward include the surface modification and the improvement of the electron mobility of the TiO_2 work electrode, such as the suppression of charge recombination by depositing an oxide layer on TiO_2 or adding saturated alkyl tail

Received: April 16, 2013
Accepted: June 20, 2013
Published: June 20, 2013

to dyes or using interfacial organic molecules like 4-tert-butylpyridine (TBP).[9−14] A striking expample is the use of TBP to improve the V_{oc} of DSCs from 0.38 to 0.72 V.[15] But most of these methods usually do not work so well for the overall efficiency of DSCs. Though the V_{oc} value may be increased, the overall efficiency is not high. For instance, a V_{oc} value of 0.87 V was observed when Ta-doped TiO_2 nanowire array was used for DSCs.[10] But the PCE is only 4.1%. Chandiran et al. observed a V_{oc} of 1.1 V by depositing a thin layer of Ga_2O_3 on TiO_2 for DSCs with Co complexes as the redox species, while they found that the PCE was lower than 4% due to the low J_{sc}.[11] V_{oc} as high as 0.84 V was attained by using ZnSe to suppressing the charge recombination, but the PCE was only 4.5%.[16] In order to improve the V_{oc}, various redox species, particularly metal complexes, with a E_{redox} lower than I^-/I_3^- were investigated for DSCs,.[11,17−20] The best examples are Co complexes, which can give rise to a V_{oc} of 0.94 V and a PCE of more than 12% under AM1.5 illumination.[7] However, other redox species are not so successful in improving the overall PCE of DSCs. For instance, when Br^-/Br_3^- were employed as the redox species, the V_{oc} could be as high as 1.15 V, whereas the photovoltaic efficiency was only 3.7%.[18]

The regeneration of the redox species on the counter electrode can also affect the V_{oc} value of DSCs. V_{oc} can be improved by reducing the overpotential for the reduction of the redox species on the counter electrode. But this has been rarely explored. Although many materials have been investigated as the counter electrode of DSCs, the purposes are to lower the cost of the counter electrode by reducing the Pt loading[21,22] or developing Pt-free materials, such as carbon black,[23,24] conducting polymer,[25−29] carbon nanotube,[30−32] graphene,[33−43] composites of carbon nanotube and graphene,[44−48] and nitrides.[49] These Pt-free materials can effectively catalyze the electrochemical redox of iodide/triiodide, but the corresponding DSCs usually exhibit lower PCEs than the control DSCs with Pt by pyrolysis as the counter electrode. In addition, the Pt-free counter electrodes usually do not improve the V_{oc} value of DSCs. Although high V_{oc} values are sometimes observed when Pt-free materials are used as the counter electrode, the current density becomes so low that the DSCs actually exhibit remarkably lower PCEs in comparison with the control devices with Pt as the counter electrode.

In this paper, we report the significant improvement in both V_{oc} and PCE of DSCs by using gel-coated composites of reduced graphene oxide (rGO) and single-walled carbon nanotubes (SWCNTs) as the counter electrode. The rGO-SWCNT (rGS) composites were prepared through the gel formation of rGO and SWCNTs with liquid polyethylene glycol (PEG) and subsequent removal of PEG by heating. RGS can effectively catalyze the reduction of triiodide. The optimal V_{oc} value is 0.86 V for fresh I^-/I_3^- DSCs with rGS as the counter electrode. It further increases to 0.90 V after aging for one week. Both V_{oc} and PCE of the DSCs with the rGS counter electrode are remarkably higher than those of the control DSCs with Pt by pyrolysis as the counter electrode, which has been regarded as the most effective counter electrode for I^-/I_3^- DSCs.

2. EXPERIMENTAL SECTION

2.1. Materials. Nature graphite flake (purity: 99.8%, ~325 mesh) was obtained from Alfa Aesar. SWCNTs produced by chemical vapor deposition (CVD) were purchased from Carbon Solution in USA. The SWCNTs had a purity of >90%, outer diameter of 1−2 nm, inner diameter of 0.8−1.6 nm, length of 5−30 μm, and specific surface area of >380 $m^2\ g^{-1}$. TiO_2 pastes (DSL 18NR-T and WER2-O45 Reflector) were supplied by Dyesol. Cis-diisothiocyanate-bis (2,2-bipyridyl-4,4-dicarboxylate) ruthenium(II) bis(tetrabutylammonium) (N719), fluorine-doped tin oxide (FTO) glass and Surlyn films were purchased from Solaronix. Zn powder was supplied by Riedel-de Haen. All the other chemicals, including PEG (molecular weight ≈200 g mol^{-1}), iodine, 1-propyl-3-methyl-imidazolium iodide (PMII), guanidinium thiocyanate, TBP, lithium iodide, tetrabutylammonium hexafluorophosphate, titanium tetrachloride, chloroplatinic acid, sodium nitrate, potassium permanganate, sulfuric acid (concentration >98%), hydrogen peroxide, acetonitrile, and tertbutanol were purchased from Sigma-Aldrich. All the chemicals were used as received.

2.2. Preparation of rGS/PEG Gels and rGS Films. RGO was prepared through the chemical oxidation of graphite and subsequent reduction of graphene oxide with Zn powder as described in our previous reports.[50,51] SWCNT/PEG gels were prepared by mixing SWCNTs with PEG under ultrasonication by a Sonics & Materials Vibracll VC 505 ultrasonic dispenser for 20 min.[31,54] 5 mg SWCNTs were dispersed in 2 mL of PEG. RGO/PEG gels were formed by dispersing rGO in PEG in an agate mortar by mechanical grinding for 20 min.[35] Five milligrams of rGO was dispersed in 2 mL of PEG. An rGO/SWCNT gel was prepared by mixing a SWCNT gel with an rGO gel and subsequently mechanically grinding the mixture for 30 min. The total amount of SWCNTs and rGO was 5 mg in 10 mL of PEG.

RGS films on FTO glass were fabricated by gel coating. RGS/PEG gels were coated on FTO glass by doctor blade. They were heated at 200 °C for 5 min. Then, the heating temperature was gradually increase to 430 °C at a rate of 10 °C per min. RGS films were obtained after further heating at 430 °C for 5 min. RGO and SWCNTs films on FTO glass were fabricated through the similar gel-coating procedure.

2.3. Fabrication and Characterization of DSCs. The DSCs were fabricated through a similar procedure reported in literature.[52,53] The anode was a layer of mesoporous TiO_2 (12 μm-thick Dyesol DSL 18NR-T and 3 μm-thick WER2−0 Reflector) on FTO glass. It was sintered at 325 °C for 5 min, 375 °C for 5 min, 450 °C for 15 min, and 500 °C for 15 min. It was then soaked in 0.04 M $TiCl_4$ aqueous solution for 30 min, rinsed with water and ethanol, and subsequently sintered at 500 °C for 35 min. After the mesoporous TiO_2 films were cooled to 80 °C, they were soaked in 0.5 mM N719 of acetonitrile/tertbutanol (volume ratio = 1:1) solution for 20 h. This photoanode was assembled with a counter electrode with two or three layers hot-melt Surlyn film (25 μm thick per layer) between them. Different materials, including Pt, rGO, SWCNTs and rGS composites, on FTO glass were used as the counter electrodes. Pt was deposited on FTO glass as the counter electrode by pyrolysis of 0.2 M H_2PtCl_6 ethanol solution at 400 °C for 15 min. The cells were filled with an electrolyte containing 0.6 M PMII, 0.03 M I_2, 0.1 M guanidinium thiocyanate and 0.5 M TBP in acetonitrile/valeronitrile (volume ratio = 17:3).

The photovoltaic performance of DSCs was measured with a computer-programmed Keithley 2400 source/meter under AM1.5G illumination (100 mW cm^{-2}) by a Newport's Oriel class A solar simulator, which was certified to the JIS C 8912 standard. A circular mask with a diameter of 5.2 mm was placed on each DSC during the photovoltaic tests. DSCs were stored in dark in ambient conditions for the aging tests.

2.4. Characterization of Materials. Thermogravimetric analytical (TGA) curves were acquired with a TA SDT Q600. Scanning electron microscopic (SEM) images were taken with a Zeiss Supra 40 FE SEM. Transmission electron microscopic (TEM) images were collected with a JEOL JEM 2010F transmission electron microscope equipped with a field emission gun. The thicknesses were determined using a P-10 Alpha-Step profiler by Tencor. Conductivitess were measured by the four-point probe method with a Keithley 2400 source/meter. Electrochemical impedance spectroscopy (EIS) and cyclic voltammetry (CV) were carried out with a PGSTAT302N+FRA2 electrochemical system by Autolab. EIS was performed on symmetric cells with various materials on FTO glass as the two electrodes. The frequency was from 200 000 down to 0.05 Hz, and the amplitude was 10 mV. The electrolyte of the symmetric cells was the same as that for

DSCs. CV was excuted in acetonitrile solution consisted of 5 mM LiI, 0.25 mM I_2, and 0.1 M$(C_4H_9)_4NPF_6$. RGS, Pt, rGO, and SWCNTs on FTO were used as the working electrodes. A Pt foil and a Ag/Ag^+ electrode were used as the counter and reference electrodes, respectively.

3. RESULTS AND DISCUSSION

3.1. Photovoltaic Performance of DSCs with rGS as the Counter Electrode. The rGS composites were prepared by gel formation and gel coating. Both rGO and SWCNTs can form gels with liquid PEG.[31,36,54,55] The rGO/PEG gels were formed by dispersing rGO in PEG via mechanical grinding, and the SWCNT/PEG gels were prepared by dispersing SWCNTs in PEG under ultrasonication. The gel formation is due to the formation of the solid networks of SWCNTs or rGO and the van der Waals interactions between SWCNTs or rGO and PEG that is a surfactant. An rGS/PEG gel was formed by mixing an rGO/PEG gel with a SWCNT/PEG gel. The rGS/PEG gels were coated on FTO glass by doctor blade, and binder-free rGS films were obtained by heating the rGS/PEG gels up to 430 °C. As indicated in Figure 1, PEG can be completely removed by heating up to 430 °C in air, whereas there is hardly any weight loss for SWCNTs and rGO below 430 °C.[56]

The gel-coated binder-free rGS films are conductive. The conductivity increases with the increase of the SWCNT loading in the composites (Figure 2). This is attributed to the higher conductivity of SWCNTs than rGO. The conductivity of rGO by gel coating is 33 S cm^{-1}, whereas the conductivity of SWCNTs by gel coating is 320 S cm^{-1}. The conductivity of the gel-coated rGO films is lower than that of the rGO films prepared by filtration of rGO aqueous solution as report in our previous papers because the gel-coated rGO films are more porous than those by filtration.[50,51]

The rGS films had good adhesion to FTO glass. The FTO glasses coated with rGS were used as the counter electrode of DSCs. Figure 3 presents the current density (J)−voltage (V) curve of a fresh DSC with a composite film of 80 wt % rGO−20 wt % SWCNT (rGS-20) that is 15 μm thick as the counter electrode. The device architecture is shown in the inset of Figure 3. The $J-V$ curves of control DSCs with Pt fabricated by pyrolysis of H_2PtCl_6 on FTO glass, gel-coated rGO, and gel-coated SWCNTs as the counter electrode, are also presented for comparison. The rGO and SWCNT films have the same thickness of 15 μm as the rGS-20 films. The photovoltaic

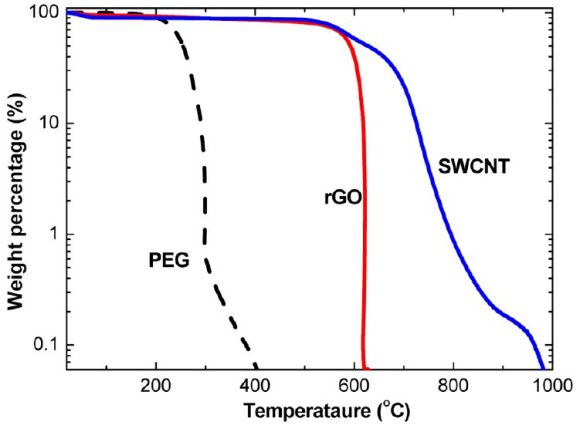

Figure 1. TGA curves of PEG, rGO, and SWCNTs.

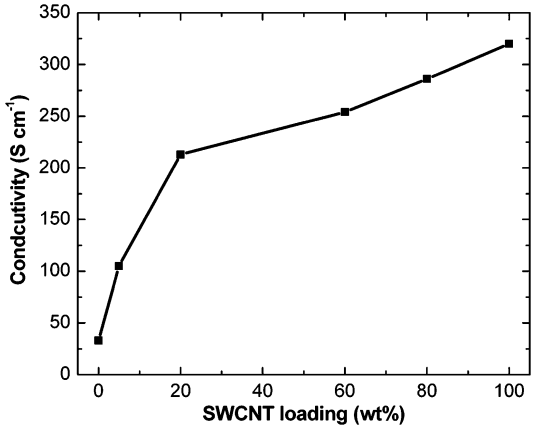

Figure 2. Variation in the conductivity of rGS composites with the SWCNT loading.

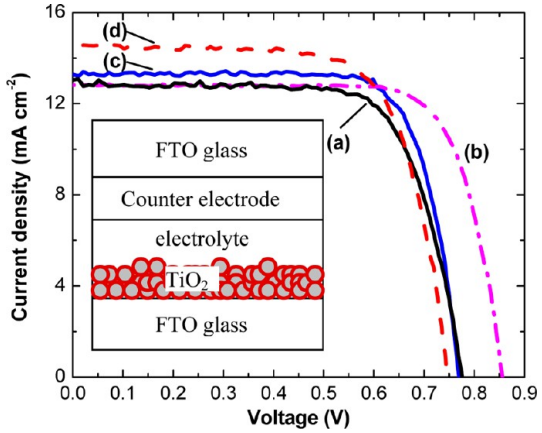

Figure 3. $J-V$ curves of fresh DSCs with different materials as the counter electrode. (a) rGO, (b) rGS-20, (c) Pt, and (d) SWCNTs. The inset is the schematic structure of the DSCs.

Table 1. Photovoltaic Parameters of DSCs with rGO, rGS-20, SWCNTs, and Pt as the Counter Electrode

counter electrode	V_{oc} (V)	J_{sc} (mA cm^{-2})	FF	PCE (%)
rGO	0.78	12.82	0.72	7.19
rGS-20	0.86	12.81	0.76	8.37
SWCNTs	0.75	14.56	0.71	7.75
Pt	0.77	13.31	0.76	7.79

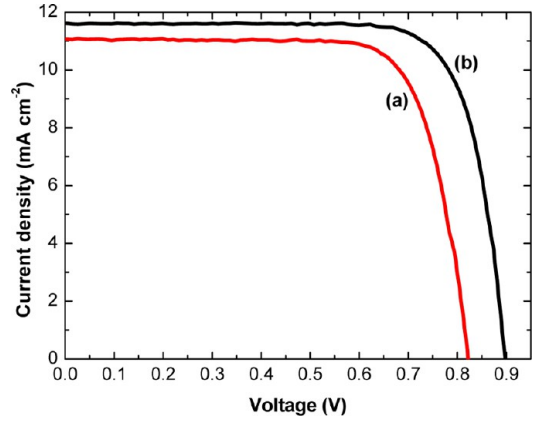

Figure 4. $J-V$ curves of DSCs with (a) Pt and (b) rGS-20 as the counter electrode after 7 days.

dx.doi.org/10.1021/am401392k | ACS Appl. Mater. Interfaces 2013, 5, 6657−6664

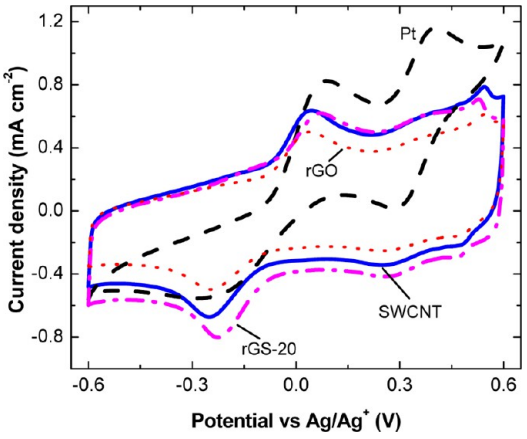

Figure 5. CVs of I^-/I_3^- with rGO, SWCNTs, rGS-20, and Pt as the working electrodes.

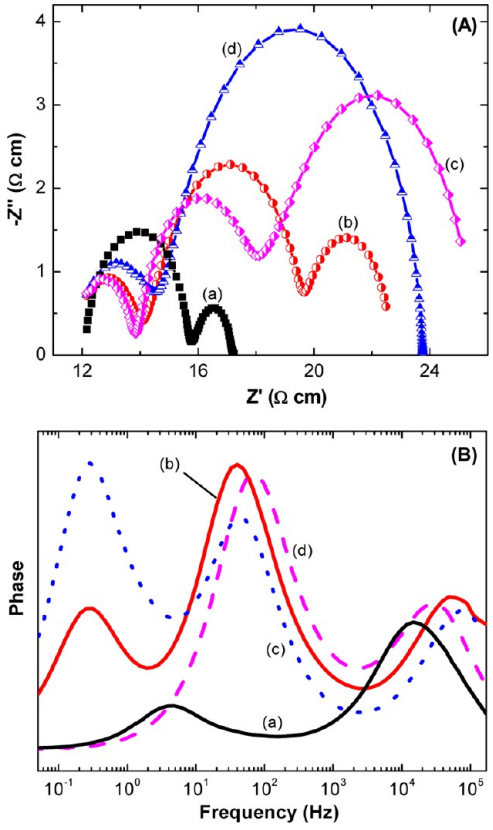

Figure 6. (A) Nyquist plots and (B) Bode plots of symmetrical cells with two FTO glass sheets coated with (a) Pt, (b) rGS-20, (c) SWCNTs, and (d) rGO as the electrodes.

parameters, including J_{sc}, V_{oc}, fill factor (FF), and PCE, of these DSCs are summarized in Table 1. The PCE (8.37%) of the DSC with rGS-20 is remarkably higher than those of control DSCs with Pt (7.79%), rGO (7.19%), and SWCNTs (7.75%) as the counter electrode. The increase in the PCE is ascribed to the increase in V_{oc}. The DSC with rGS-20 exhibits a V_{oc} of 0.86 V, whereas the V_{oc} values of other DSCs are below 0.80 V.

The photovoltaic performance of DSCs with rGS as the counter electrode depends on the loading of SWCNTs in the composite. The $J-V$ curves of DSCs with rGS composites of other SWCNT loadings, 5, 10, 30, 40, 60, and 80 wt %, are presented in Figure S1 in the Supporting Information. These rGS films also have a thickness of 15 μm. Figure S2 in the Supporting Information illustrates the variations in V_{oc}, J_{sc}, FF, and PCE of DSCs with the SWCNT loading of rGS. All the rGS composites give rise to V_{oc} values higher than 0.8 V, but the V_{oc} value of the DSCs with rGS-20 is the highest. In terms of the V_{oc}, FF, and PCE of the DSCs, the optimal SWCNT loading is 20 wt % for rGS.

The V_{oc} value of the DSCs with rGS as the counter electrode increases with time. As shown in Figure 4, the V_{oc} value reaches 0.90 V after 7 days. In contrast, the V_{oc} value of the control DSC with Pt is only 0.82 V. To the best of our knowledge, this is the first time to observe such a high V_{oc} value for highly efficient I^-/I_3^- DSCs by simply using a different counter electrode. Our approach to increase the V_{oc} of DSCs is significantly different from other methods reported in literature, such as suppression of the charge recombination between the work electrode and the electrolyte and adoption of redox species with low redox potential.[9−14,17−20]

Though composites of graphene and carbon nanotubes were investigated as the counter electrode of DSCs, the DSCs exhibited PCEs remarkably lower than control DSCs with Pt as the counter electrode.[44−48] Choi et al. fabricated composites of graphene and multiwalled carbon nanotubes (MWCNTs) by growing MWCNTs on chemical reduced graphene layers via chemical vapor deposition and investigated their application as the counter electrode of DSCs.[44,45] The DSCs exhibited a PCE of 3.0 or 4.46% depending the method for the composition fabrication. Zhu et al. synthesized rGO-MWCNT composites by the electrophoretic deposition for the counter electrode of DSCs.[46] The highest PCE for their DSCs was 6.17%. Battumur et al. prepared graphene-MWCNT composites by doctor blade and observed an optimal efficiency of 4.0%.[47] Velten et al. drop-casted graphene onto MWCNTs and studied the graphene-MWCNT composites as the counter electrode of DSCs.[48] The optimal PCE of their DSCs was 7.55%. All the V_{oc} and PCE values of the DSCs with graphene-MWCNT composites are lower than the control DSCs with Pt by pyrolysis as the counter electrode. The high PCE of our DSCs with rGS-20 can be attributed to the exploitation of SWCNTs in rGS and the gel-coating method. As we reported before, gel-coated SWCNT films as the counter electrode can give rise to high photovoltaic performance for DSCs, better than that with gel-coated MWCNT films as the counter electrode.[31]

The V_{oc} value of our DSCs with rGS as the counter electrode is also remarkably higher than those with graphene as the counter electrode.[33−43] For example, Kavan et al. found that graphene nanoplateletes can outperform Pt as the counter electrode of DSCs with Co complexes as the redox species.[33] But the V_{oc} is lower than that of DSCs with Pt as the counter electrode. Various carbon materials were investigated as the counter electrode of DSCs by Wu et al.[57] The V_{oc} is lower than 0.81 V, V_{oc} and PCE are lower than those of DSCs with Pt as the counter electrode. Graphene was also blended into the TiO_2 photoanode of DSCs.[58−60] But no increase in V_{oc} was observed.

3.2. Mechanism for the High V_{oc} of DSCs with rGS as the Counter Electrode. The high photovoltaic performance of the DSCs with rGS as the counter electrode is related to the electrocatalysis of rGO and SWCNTs.[61,62] Presumably, the high V_{oc} of DSCs with rGS as the counter electrode is related to the reduction in the overpotential for the I_3^- reduction on the counter electrode, because these devices are different from the control devices with Pt, rGO or SWCNTs as the counter

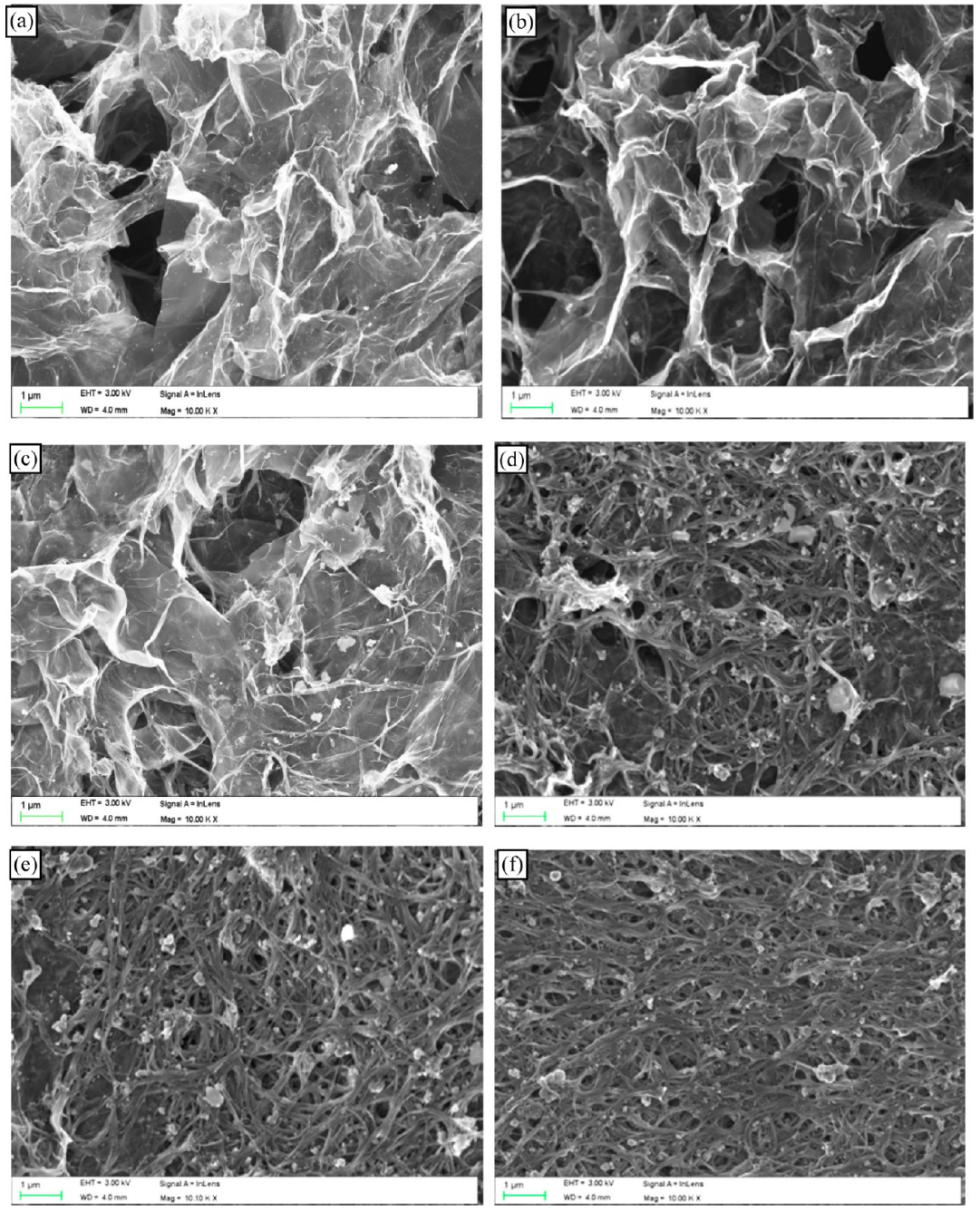

Figure 7. SEM images of (a) rGO, (b) rGS-5, (c) rGS-20, (d) rGS-60, (e) rGS-80, and (f) SWCNTs.

electrode only in the counter electrode. The redox behavior of I^-/I_3^- was investigated by CV. Pt, rGS-20, rGO and SWCNTs on FTO glasses were used as the working electrodes for the CVs. As shown in Figure 5, there are two oxidation/reduction pairs in the potential range from −0.6 to 0.6 V vs Ag/Ag^+. The pair at the low potential range are the redox of iodide/triiodide, $I_3^- + 2e^- \leftrightarrow 3I^-$, and the other pair at the high potential range correspond to the redox of iodine/triiodide $3I_2 + 2e^- \leftrightarrow 2I_3^-$.[63] The redox of the first pair is the regeneration of the redox species on the counter electrode of DSCs.[64] The CV demonstrates that rGS-20 can effectively catalyze the redox of I^-/I_3^-.[65] The reduction peak potentials of the I_3^- reduction are −0.248, −0.224, −0.250, and −0.253 V vs Ag/Ag^+ for rGO, rGS-20, SWCNTs and Pt as the working electrodes, respectively. The reduction peak potential of I_3^- on rGS-20 is higher than on other materials. These reduction potentials are roughly consistent with the V_{oc} values of the DSCs with these materials as the counter electrode. Hence, the high V_{oc} value of DSCs with rGS-20 can be attributed to the decrease in the overpotential for the I_3^- reduction.

The redox behavior of I^-/I_3^- was also investigated by CV using rGS composites with SWCNT loadings of 5, 60, and 80 wt % on FTO as the working electrodes (see Figure S3 in the Supporting Information). The I_3^- reduction peak potentials are −0.246, −0.170, and −0.226 V vs Ag/Ag^+ for rGS-5, rGS-60, and rGS-80 as the working electrodes, respectively. Thus, there is an optimal rGO-to-SWCNT composition for the reduction of I_3^-. These potentials roughly agree with the V_{oc} values of the DSCs with rGS composites of different SWCNT loadings as the counter electrode.

dx.doi.org/10.1021/am401392k | ACS Appl. Mater. Interfaces 2013, 5, 6657−6664

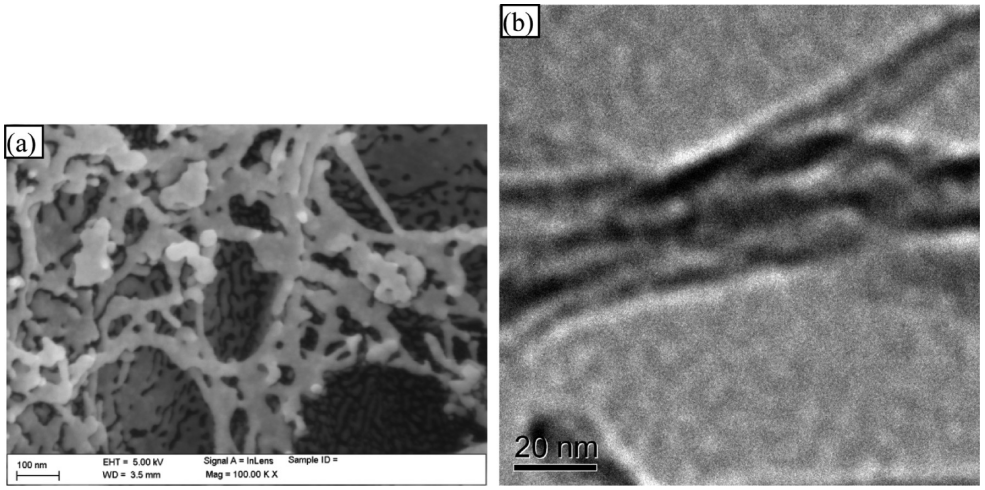

Figure 8. (a) High-resolution SEM and (b) TM images of rGS-20.

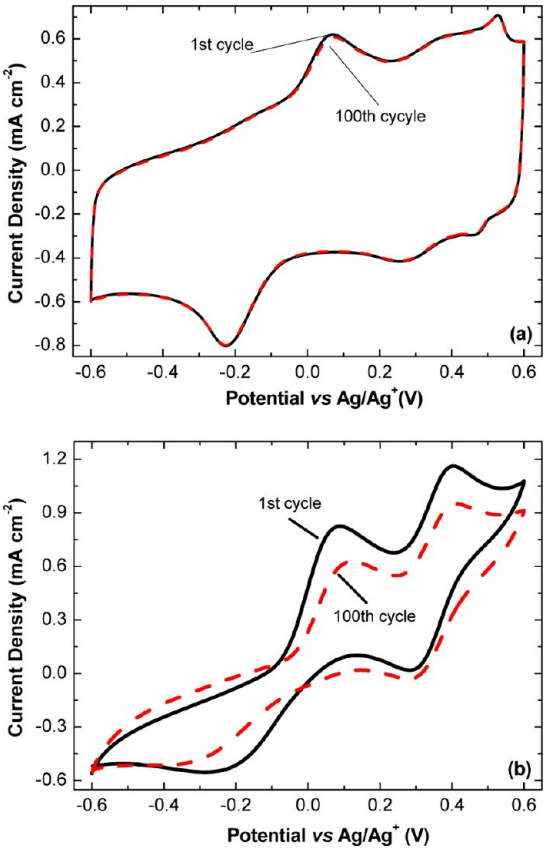

Figure 9. 1st and 100th CVs of I^-/I_3^- with (a) rGS-20 and (b) Pt as the working electrodes.

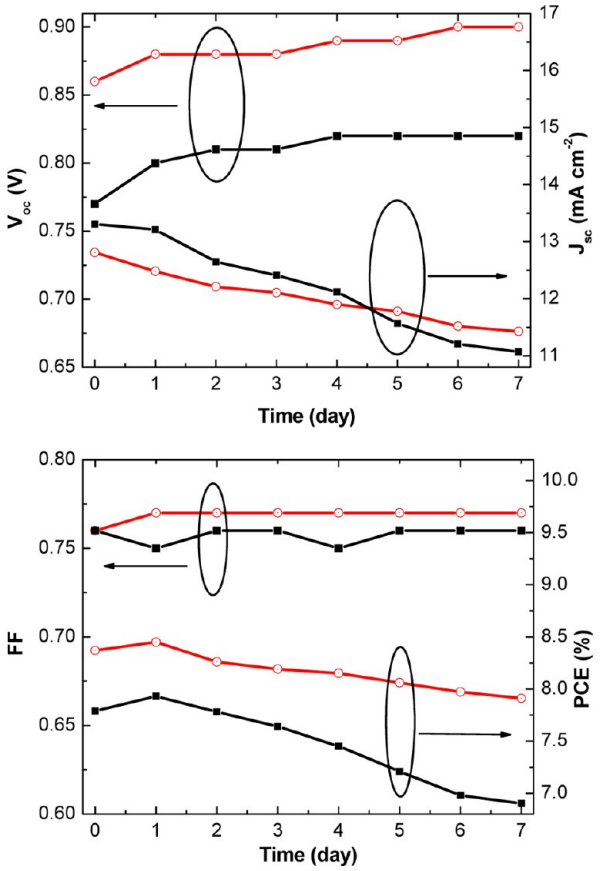

Figure 10. Aging tests of DSCs with rGS-20 (open circles) and Pt (solid squares) on FTO as the counter electrodes.

In order to further understand the high V_{oc} of DSCs with rGS-20, electrochemical impedance spectroscopy (EIS) was carried out to study symmetrical cells with two FTO sheets deposited with rGS-20, rGO, SWCNTs, or Pt as the two electrodes. The cells were filled with the same electrolyte as for DSCs. Panels A and B in Figure 6 show the Nyquist and Bode plots, respectively. There are two semicircles for the cells with Pt or rGO as the electrodes. The one in the high-frequency region is due to the charge transfer between the electrolyte and the electrodes, and the other at the low frequency region is attributed to the diffusion of redox species in the electrolyte.[66]

In contrast, there are three semicircles when SWCNTs or rGS-20 are used as the electrode. The additional semicircle appears at the low frequency range of less than 5 Hz. The semicircle in the low frequency range can be attributed to the diffusion of the redox species through the SWCNT or rGS-20 films. This semicircle does not appear for the cells with Pt or rGO as the electrodes, because Pt and rGO can be considered as two-dimensional planar electrodes and the ion diffusion through these electrodes is much less significant than along the electrolyte.

dx.doi.org/10.1021/am401392k | *ACS Appl. Mater. Interfaces* 2013, 5, 6657−6664

The assignment for the process in the low-frequency range is also evidenced by the EIS results of the symmetrical cells with rGS composites of different SWCNT loadings (see Figure S4 in the Supporting Information). The semicircle in the low frequency is not remarkable for rGS-5, and it becomes more significant with the increase in the SWCNT loading in rGS, that is, the resistance for the diffusion of the redox species in the electrode increases.

The CV and EIS results suggest that rGS can be more effective in catalyzing the I_3^- reduction than Pt, rGO and SWCNTs. RGO and SWCNTs are prepared by the same gel formation and gel coating process as rGS, so that the reason for the high electrocatalytic activity cannot be attributed to any possible oxidation of rGO and SWCNTs during the heating process. The high electrocatalytic activity of rGS can be ascribed to the synergetic effects of SWCNTs and rGO. RGO can have high electrocatalytic activity arising from its high specific surface area, whereas SWCNTs give rise to high conductivity for rGS composites and facilitate the penetration of the redox species into the rGO sheets. In the absence of SWCNTs, rGO has low conductivity and low effective surface area for the electrochemical reduction due to the agglomeration of rGO sheets. Both factors lead to the low electrocatalytic activity for rGO. On the other hand, when SWCNTs or rGS with a high SWCNT loading are used as the counter electrode, the resistance for the ion diffusion through the counter electrode is so high that the electrocatalytic activity becomes not high as well.

The discussion above suggests that the ion diffusion through rGS is related to its morphology. Figure 7 presents the SEM images of rGO, RGS-5, rGS-20, rGS-60, rGS-80, and SWCNTs. There are large pores for rGO, whereas small pores appear for rGS. The small pores are due to the presence of SWCNTs. They can facilitate the diffusion of the redox species into rGS.[67−69] In addition, the SEM images indicate that SWCNTs are well dispersed in rGS, so that they can bridge the rGO sheets and improve the charge transport.

Presumably, the interaction between SWCNTs and rGO is crucial for the synergetic effects of SWCNTs and rGO. There should be strong $\pi-\pi$ coupling between SWCNTs and rGO because both of them have the conjugated C=C bonds.[70,71] But it is difficult to detect the interactions by spectroscopy. The interaction between SWCNTs and rGO sheets were further investigated by high-resolution SEM and TEM (Figure 8). The SWCNT bundles do not have very clear shape but have blur edge. This is probably due to the attachment of rGO sheets on SWCNTs.

The rGS composites also have better stability than Pt in catalyzing the redox of I^-/I_3^-. As shown in Figure 9a, no appreciable change was observed for the electrochemical activity of I^-/I_3^- after 100 cycles, when rGS-20 was used as the working electrode. In contrast, the electrochemical activity became remarkably low after 100 cycles, when Pt was employed as the working electrode (Figure 9b).

Aging tests were carried out for DSCs with rGS-20 and Pt as the counter electrodes (Figure 10). Besides the counter electrode, other factors such as the sealing of the cells can also affect the aging stability. But the aging test can still provide useful information related to the counter electrode of DSCs. The DSC with rGS-20 as the counter electrode is more stable than that with Pt as the counter electrode. This is because Pt degrades in the electrolyte, whereas SWCNTs and rGO are quite stable in the electrolyte.[31,35,72]

4. CONCLUSIONS

Gel-coated rGS composites can outperform Pt, rGO, and SWCNTs in catalyzing the reduction of I_3^- and functioning as the counter electrode of DSCs. The electrocatalytic activity depends on the SWCNT loading of rGS, and the optimal SWCNT loading is 20 wt %. RGS composites were investigated as the counter electrode of DSCs. RGS-20 can give rise to a V_{oc} of 0.86 V and PCE of 8.37% for fresh DSCs, significantly higher than those (V_{oc} = 0.77 V, PCE = 7.79%) of the control DSCs with Pt fabricated by pyrolysis as the counter electrode. The V_{oc} value of DSCs with rGS-20 further increases to 0.90 V after one week. The high electrocatalytic activity of rGS on the I_3^- reduction is ascribed to the synergetic effects of rGO and SWCNTs. RGO can have high electrocatalytic activity arising from its high specific surface area, whereas SWCNTs give rise to high conductivity for rGS and facilitate the penetration of the redox species into the rGO sheets.

■ ASSOCIATED CONTENT

Supporting Information

Additional figures (PDF). This material is available free of charge via the Internet at http://pubs.acs.org.

■ AUTHOR INFORMATION

Corresponding Author

*E-mail: mseoj@nus.edu.sg. Fax: +65 6776 3604. Tel: +65 6516 1472.

Author Contributions

§Authors H.Z. and C.Y.N. contributed equally to this work

Notes

The authors declare no competing financial interest.

■ ACKNOWLEDGMENTS

This research work was financially supported by a research grant from the Ministry of Education, Singapore (R-284-000-106-112). H.Q.Z. thanks the student exchange program between the National Unviersity of Singapore and Tongji University in China.

■ REFERENCES

(1) Gratzel, M. *Acc. Chem. Res.* **2009**, *42*, 1788−1798.
(2) Joshi, P.; Zhang, L.; Chen, Q.; Galipeau, D.; Fong, H.; Qiao, Q. *ACS Appl. Mater. Interf.* **2010**, *2*, 3572−3577.
(3) Tétreault, N.; Grätzel, M. *Energy Environ. Sci.* **2012**, *5*, 8506−8516.
(4) Hardin, B. E.; Snaith, H. J.; McGehee, M. D. *Nat. Photon.* **2012**, *6*, 162−169.
(5) Snaith, H. J. *Adv. Funct. Mater.* **2010**, *20*, 13−19.
(6) Chiang, Y. F.; Chen, R. T.; Shen, P. S.; Chen, P.; Guo, T. F. *J. Power Sources* **2013**, *225*, 257−262.
(7) Yella, A.; Lee, H. W.; Tsao, H. N.; Yi, C.; Chandiran, A. K.; Nazeeruddin, Md. K.; Diau, E. W. G.; Yeh, C. Y.; Zakeeruddin, S. M.; Grätzel, M. *Science* **2011**, *334*, 629−634.
(8) Raga, S. R.; Barea, E. M.; Fabregat-Santiago, F. *J. Phys. Chem. Lett.* **2012**, *3*, 1629−1634.
(9) Zhang, Z. P.; Zakeeruddin, S. M.; O'Regan, B. C.; Humphry-Baker, R.; Gratzel, M. *J. Phys. Chem. B* **2005**, *109*, 21818−21824.
(10) Feng, X.; Shankar, K.; Paulose, M.; Grimes, C. A. *Angew. Chem., Int. Ed.* **2009**, *48*, 8095−8098.
(11) Chandiran, A. K.; Tetreault, N.; Humphry-Baker, R.; Kessler, F.; Baranoff, E.; Yi, C.; Nazeeruddin, M. K.; Grätzel, M. *Nano Lett.* **2012**, *12*, 3941−3947.
(12) Xu, J.; Wu, H.; Jia, X.; Zou, D. *Chem. Commun.* **2012**, *48*, 7793−7795.

(13) Tetreault, N.; Arsenault, E.; Heiniger, L. P.; Soheilnia, N.; Brillet, J.; Moehl, T.; Zakeeruddin, S.; Ozin, G. A.; Gratzel, M. *Nano Lett.* **2011**, *11*, 4579−4584.
(14) Neo, C. Y.; Ouyang, J. *J. Power Sources* **2011**, *196*, 10538−10542.
(15) Nazeeruddin, M. K.; Kay, A.; Rodicio, I.; Humpbry-Baker, R.; Muller, E.; Liska, P.; Vlachopoulos, N.; Gratzel, M. *J. Am. Chem. Soc.* **1993**, *115*, 6382−6390.
(16) Xu, J.; Yang, X.; Yang, Q. D.; Wong, T. L.; Lee, S. T.; Zhang, W. J.; Lee, C. S. *J. Mater. Chem.* **2012**, *22*, 13374−13379.
(17) Stergiopoulos, T.; Falaras, P. *Adv. Energy Mater.* **2012**, *2*, 616−627.
(18) Teng, C.; Yang, X.; Yuan, C.; Li, C.; Chen, R.; Tian, H.; Li, S.; Hagfeldt, A.; Sun, L. *Org. Lett.* **2009**, *11*, 5542−5545.
(19) Bai, Y.; Yu, Q.; Cai, N.; Wang, Y.; Zhang, M.; Wang, P. *Chem. Commun.* **2011**, *47*, 4376−4378.
(20) Iwamoto, S.; Sazanami, Y.; Inoue, M.; Inoue, T.; Hoshi, T.; Shigaki, K.; Kaneko, M.; Maenosono, A. *ChemSusChem* **2008**, *1*, 401−403.
(21) Papageorgiou, N.; Maier, W. F.; Gratzel, M. *J. Electrochem. Soc.* **1997**, *144*, 876−884.
(22) Cho, S. J.; Neo, C. Y.; Mei, X.; Ouyang, J. *Electrochim. Acta* **2012**, *85*, 16−24.
(23) Murakami, T. N.; Ito, S.; Wang, Q.; Nazeeruddin, M. K.; Bessho, T.; Cesar, I.; Liska, P.; Humphry-Baker, R.; Comte, P.; Pechy, P.; Gratzel, M. *J. Electrochem. Soc.* **2006**, *153*, A2255−A2261.
(24) Imoto, K.; Takahashi, K.; Yamaguchi, T.; Komura, T.; Nakamura, J. I.; Murata, K. *Sol. Energy Mater. Sol. Cells* **2003**, *79*, 459−469.
(25) Fan, B. H.; Mei, X.; Sun, K.; Ouyang, J. *Appl. Phys. Lett.* **2008**, *93*, 143103(1)−143103(3).
(26) Huang, K. C.; Hu, C. W.; Tseng, C. Y.; Liu, C. Y.; Yeh, M. H.; Wei, H. Y.; Wang, C. C.; Vittal, R.; Chu, C. W.; Ho, K. C. *J. Mater. Chem.* **2012**, *22*, 14727−14733.
(27) Burschka, J.; Brault, V.; Ahmad, S.; Breau, L.; Nazeeruddin, M. K.; Marsan, B.; Zakeeruddin, S. M.; Grätzel, M. *Energy Environ. Sci* **2012**, *5*, 6089−6097.
(28) Hong, W.; Xu, Y.; Lu, G.; Li, C.; Shi, G. *Electrochem. Commun.* **2008**, *10*, 1555−1558.
(29) Brennan, L. J.; Byrne, M. T.; Bari, M.; Gun'ko, Y. K. *Adv. Energy Mater.* **2011**, *1*, 472−485.
(30) Lee, W. J.; Ramasamy, E.; Lee, D. Y.; Song, J. S. *ACS Appl. Mater. Interfaces* **2009**, *1*, 1145−1149.
(31) Mei, X. G.; Cho, S. J.; Fan, B. H.; Ouyang, J. *Nanotechnology* **2010**, *21*, 395202(1)−395202(9).
(32) Cha, S. I.; Koo, B. K.; Seo, S. H.; Lee, D. Y. *J. Mater. Chem.* **2010**, *20*, 659−662.
(33) Kavan, L.; Yum, J. H.; Grätzel, M. *Nano Lett.* **2011**, *11*, 5501−5506.
(34) Kavan, L.; Yum, J. H.; Nazeeruddin, M. K.; Grätzel, M. *ACS Nano* **2011**, *5*, 9171−9178.
(35) Zheng, H. Q.; Neo, C. Y.; Mei, X. G.; Qiu, J.; Ouyang, J. *J. Mater. Chem.* **2012**, *22*, 14465−14474.
(36) Zhang, D. W.; Li, X. D.; Li, H. B.; Chen, S.; Sun, Z.; Yin, X. J.; Huang, S. M. *Carbon* **2011**, *49*, 5382−5388.
(37) Kavan, L.; Yum, J. H.; Gratzel, M. *ACS Nano* **2011**, *5*, 165−172.
(38) Roy-Mayhew, J. D.; Bozym, D. J.; Punckt, C.; Aksay, I. A. *ACS Nano* **2010**, *4*, 6203−6211.
(39) Roy-Mayhew, J. D.; Boschloo, G.; Hagfeldt, A.; Aksay, I. A. *ACS Appl. Mater. Interfaces* **2012**, *4*, 2794−2800.
(40) Bajpai, R.; Roy, S.; Kumar, P.; Bajpai, P.; Kulshrestha, N.; Rafiee, J.; Koratkar, N.; Misra, D. S. *ACS Appl. Mater. Interfaces* **2011**, *3*, 3884−3889.
(41) Kavan, L.; Yum, J. H.; Graetzel, M. *ACS Appl. Mater. Interfaces* **2012**, *4*, 6999−7006.
(42) Jang, S. J.; Kim, Y. G.; Kim, D. Y.; Kim, H. G.; Jo, S. M. *ACS Appl. Mater. Interfaces* **2012**, *4*, 3500−3507.
(43) Tjoa, V.; Chua, J.; Pramana, S. S.; Wei, J.; Mhaisalkar, S. G.; Mathews, N. *ACS Appl. Mater. Interfaces* **2012**, *4*, 3447−3452.
(44) Choi, H.; Kim, H.; Hwang, S.; Choi, W.; Jeon, M. *Sol. Energy Mater. Sol. Cells* **2011**, *95*, 323−325.
(45) Choi, H.; Kim, H.; Hwang, S.; Kang, M.; Jung, D. W.; Jeon, M. *Scr. Mater* **2011**, *64*, 601−604.
(46) Zhu, G.; Pan, L.; Lu, T.; Xu, T.; Sun, Z. *J. Mater. Chem.* **2011**, *21*, 14869−14875.
(47) Battumur, T.; Mujawar, S. H.; Truong, Q .T.; Ambade, S. B.; Lee, D. S.; Lee, W.; Han, S. H.; Lee, S. H. *Curr. Appl. Phys.* **2012**, *12*, e49−e57.
(48) Velten, J.; Mozer, A. J.; Li, D.; Officer, D.; Wallace, G.; Baughman, R.; Zakhidov, A. *Nanotechnology* **2012**, *23*, 085201(1)−085201(6).
(49) Li, G. R.; Song, J.; Pan, G. L.; Gao, X. P. *Energy Environ. Sci.* **2011**, *4*, 1680−1683.
(50) Mei, X. G.; Ouyang, J. *Carbon* **2011**, *49*, 5389−5397.
(51) Mei, X. G.; Zheng, H. Q.; Ouyang, J. *J. Mater. Chem.* **2012**, *22*, 9109−9116.
(52) Ito, S.; Chen, P.; Comte, P.; Nazeeruddin, M. K.; Liska, P.; Péchy, P.; Grätzel, M. *Prog. Photovolt. Res. Appl.* **2007**, *15*, 603−612.
(53) Neo, C. Y.; Ouyang, J. *Electrochim. Acta* **2012**, *85*, 1−8.
(54) Mei, X. G.; Ouyang, J. *Carbon* **2010**, *48*, 293−302.
(55) Mei, X. G.; Ouyang, J. *J. Mater. Chem.* **2011**, *21*, 17842−17849.
(56) Chen, H.; Müller, M. B.; Gilmore, K. J.; Wallace, G. G.; Li, D. *Adv. Mater.* **2008**, *20*, 3557−3561.
(57) Wu, M.; Lin, X.; Wang, T.; Qiu, J.; Ma, T. *Energy Environ. Sci.* **2011**, *4*, 2308−2315.
(58) Tang, Y. B.; Lee, C. S.; Xu, J.; Liu, Z. T.; Chen, Z. H.; He, Z.; Cao, Y. L.; Yuan, G.; Song, H.; Chen, L.; Luo, L.; Cheng, H. M.; Zhang, W. J.; Bello, I.; Lee, S. T. *ACS Nano* **2012**, *4*, 3482−3488.
(59) Yang, N.; Zhai, J.; Wang, D.; Chen, Y.; Jiang, L. *ACS Nano* **2010**, *4*, 887−894.
(60) Neo, C. Y.; Ouyang, J. *J. Power Sources* **2012**, *222*, 161−168.
(61) Huang, C.; Li, C.; Shi, G. Q. *Energy Environ. Sci.* **2012**, *5*, 8848−8868.
(62) Sun, Y.; Wu, Q.; Shi, G. Q. *Energy Environ. Sci.* **2011**, *4*, 1113−1132.
(63) Li, K.; Luo, Y.; Yu, Z.; Deng, M.; Li, D.; Meng, Q. *Electrochem. Commun.* **2009**, *11*, 1346−1349.
(64) Sun, H.; Luo, Y.; Zhang, Y.; Li, D.; Yu, Z.; Li, K.; Meng, Q. *J. Phys. Chem. C* **2010**, *114*, 11673−11679.
(65) Sakurai, S.; Jiang, H. Q.; Takahashi, M.; Kobayashi, K. *Electrochim. Acta* **2009**, *54*, 5463−5469.
(66) Tang, L.; Wang, Y.; Li, Y.; Feng, H.; Lu, J.; Li, J. *Adv. Funct. Mater.* **2009**, *19*, 2782−2789.
(67) Yu, D.; Dai, L. *J. Phys. Chem. Lett.* **2009**, *1*, 467−470.
(68) Neo, C. Y.; Ouyang, J. *Carbon* **2013**, *54*, 48−57.
(69) Merlet, C.; Rotenberg, B.; Madden, P. A.; Taberna, P. L.; Simon, P.; Gogotsi, Y.; Salanne, M. *Nat. Mater.* **2012**, *11*, 306−310.
(70) Zhao, M. Q.; Liu, X. F.; Zhang, Q.; Tian, G. L.; Huang, J. Q.; Zhu, W.; Wei, F. *ACS Nano* **2012**, *6*, 10759−10769.
(71) Tung, V. C.; Chen, L. M.; Allen, M. J.; Wassei, J. K.; Nelson, K.; Kaner, R. B.; Yang, Y. *Nano Lett.* **2009**, *9*, 1949−1955.
(72) Papageorgiou, N. *Coord. Chem. Rev.* **2004**, *248*, 1421−1446.